24th INTERNATIONAL CONGRESS ON SOUND AND VIBRATION
23–27 July 2017, London

ICSV24
23-27JULY 2017
LONDON CALLING

ASSESSMENT OF PERMEABLE BOUNDARY INTEGRAL FORMULATIONS FOR ROTATING BLADES NOISE PREDICTION

Federico Porcacchia
Roma Tre University, Department of Engineering, Rome, Italy
email:: federico.porcacchia@uniroma3.it

Claudio Testa, Stefano Zaghi and Roberto Muscari
CNR-INSEAN, Rome, Italy

Massimo Gennaretti
Roma Tre University, Department of Engineering, Rome, Italy

Abstract

In this work the Ffowcs Williams and Hawkings Equation for permeable surfaces (FWHE-P) is used for the prediction of the noise generated by marine propellers and horizontal-axis wind turbines. Specifically, the aim is the assessment of a boundary integral formulation that provides the acoustic pressure outside a fictitious (permeable) surface surrounding all the linear and nonlinear sources of sound generated fluid-dynamically by rotating bodies. The effects of placement and extension of this surface on predictions are investigated, dealing with the issue of the outflow disk that may be source of inaccuracy. A cylindrical surface rigidly moving (co-rotating) with the blades is chosen as the integration domain of the FWHE-P, whereas a zero-th Boundary Element Method (BEM) is used to solve the integral formulation. Steady RANS and DES tools are used to evaluate the sources of sound upon the porous surface, for a wind turbine and a propeller, respectively. Numerical investigations compare the acoustic signals given by the FWHE-P and those carried out directly by the RANS or DES simulations; the influence of the porous surface shape on the corresponding acoustic predictions is discussed.

Keywords: Acoustic Analogy, Permeable Surface Formulation, Marine Propellers Acoustics, Wind Turbines Acoustics.

1. Introduction

In many engineering applications, the noise generated by interaction of moving bodies and surrounding fluid is of great interest. Among the many theoretical and numerical models used to predict fluid-dynamically generated noise signatures, the Ffowcs Williams and Hawkings Equation (FWHE) represents a well-known and widely used approach [1]. It extends the Lighthill theory for turbulence generated sound, to account for the presence of solid moving bodies, and identifies different noise generation mechanisms that are expressed as linear monopole and dipole body surface source terms and nonlinear quadrupole field source terms within a volume of suited extension around the body.

The field sources of sound may be acoustically relevant for those configurations characterized by transonic or cavitating effects, and/or by the presence of massive turbulence or vorticity fields. The latter concerns, for instance, marine propellers which give rise to persisting, both in time and space, vortical structures, as well as wind turbines, for which noise is strongly affected by turbulent flow

structures and tip vortices: in these cases, the linear terms of the FWHE are not suitable for capturing the main characteristics of the near/far field noise [2, 3].

In this context, the use of the FWHE for porous (fictitious) surfaces (FWHE-P) surrounding the body and the corresponding field noise sources is certainly the most suitable and effective way to include the influence of field sources on noise avoiding, at the same time, cumbersome computations of volume integrals [4]. However, the requirement of accurate input data on the porous surface and the uncertainty on the evaluation of contributions from the downstream closure of the porous surface are critical issues for which a debate is still open in the literature on pros and cons and most appropriate way of application of acoustic solvers based on the FWHE-P formulation [5].

The objective of the present paper is the assessment of a boundary integral representation solving the FWH-P equation, including the issues regarding the downstream closure of the considered fictitious surface. Specifically, the acoustic analyses of a horizontal-axis wind turbine and a marine propeller in steady-state conditions are carried out, and the noise predictions from the FWHE-P-based approach are compared with those given by the CFD solver also providing the required fluid dynamic input data on the porous surface.

2. Noise Propagation Model

Under the assumption of negligible entropy changes, for $f(\mathbf{x},t)=0$ (with $|\nabla f|=1$) that identifies the points of an arbitrary (permeable) surface, S, which moves with velocity $\mathbf{v}$, the external acoustic pressure field, $p'=c_0^2\,(\rho-\rho_0)$, is governed by the following form of the Ffowcs Williams and Hawkings equation (FWHE-P) (see, for instance, [4])

$$\begin{aligned}\bar{\Box}^2 p' &= \frac{\overline{\partial}}{\overline{\partial} t}\left[\rho_0\,\mathbf{v}\cdot\nabla f\;\delta\left(f\right)\right]+\frac{\overline{\partial}}{\overline{\partial} t}\left[\rho\left(\mathbf{u}-\mathbf{v}\right)\cdot\nabla f\;\delta\left(f\right)\right]\\ &- \overline{\nabla}\cdot\left[\mathbf{P}\,\nabla f\;\delta\left(f\right)\right]-\overline{\nabla}\cdot\left[\rho\,\mathbf{u}\otimes\left(\mathbf{u}-\mathbf{v}\right)\nabla f\;\delta\left(f\right)\right]+\overline{\nabla}\cdot\overline{\nabla}\cdot\left[\mathbf{T}\,H(f)\right]\end{aligned}\tag{1}$$

where bars denote generalized differential operators, $\bar{\Box}^2=(1/c_0^2)(\overline{\partial}^2/\overline{\partial}t^2)-\overline{\nabla}^2$ represents the wave operator, whereas $H(f)$ and $\delta(f)$ are the Heaviside and Dirac delta functions, respectively. In addition, $\mathbf{u}$ is the local fluid velocity, $\mathbf{P}$ is the compressive stress tensor, $\mathbf{P}=[(p-p_0)\,\mathbf{I}+\mathbf{V}]$, with $\mathbf{V}$ representing the viscous stress tensor, and $\mathbf{T}=\left[\rho(\mathbf{u}\otimes\mathbf{u})+(p-p_0)\mathbf{I}-c_0^2(\rho-\rho_0)\mathbf{I}+\mathbf{V}\right]$ represents the Lighthill tensor.

Following the Green function approach presented in [6], in a space rigidly connected with the surface S, the boundary-field integral solution of Eq. 1 is expressed as (see also [7])

$$\begin{aligned}p'(\mathbf{x},t) &= \int_V\left[\hat{G}\,\nabla\cdot\nabla\cdot\left(\mathbf{T}\,H\right)\right]_\vartheta \mathrm{d}V(\mathbf{y})-\int_S\left[\left(\mathbf{Pn}\right)\cdot\nabla\hat{G}-\left(\mathbf{Pn}\right)^{\cdot}\cdot\nabla\vartheta\,\hat{G}\right]_\vartheta \mathrm{d}S(\mathbf{y})\\ &- \rho_0\int_S\left[\mathbf{v}\cdot\mathbf{n}\,\mathbf{v}\cdot\nabla\hat{G}+\left(\mathbf{v}\cdot\mathbf{n}\,(1-\mathbf{v}\cdot\nabla\vartheta)\right)^{\cdot}\hat{G}\right]_\vartheta \mathrm{d}S(\mathbf{y})\\ &- \int_S\left[\rho\mathbf{u}^-\cdot\mathbf{n}\,\mathbf{u}^+\cdot\nabla\hat{G}+\left(\rho\mathbf{u}^-\cdot\mathbf{n}\,(1-\mathbf{u}^+\cdot\nabla\vartheta)\right)^{\cdot}\hat{G}\right]_\vartheta \mathrm{d}S(\mathbf{y})\end{aligned}\tag{2}$$

where V is the volume surrounding (and including) the surface S where the quadrupole noise sources associated to the Lighthill stress tensor are not negligible, and $[...]_\vartheta$ indicates that the integrand must be evaluated at the retarded emission time, $\tau=t-\vartheta$, where ϑ denotes the time required by an acoustic disturbance released from a source in $\mathbf{y}$ to reach the observer point $\mathbf{x}$ at current time t.

Furthermore, $\hat{G}=-1/[4\pi\;r\,(1-M_r)]_\vartheta$ indicates the retarded Green function, with $r=|\mathbf{r}|$, $\mathbf{r}=\mathbf{x}(t)-\mathbf{y}(\tau)$, and $M_r=(\mathbf{v}\cdot\mathbf{r})/(c_0\,r)$ denotes the surface Mach number in radiation direction. In addition, the symbol $(\;)^{\cdot}$ denotes time derivation performed in the space rigidly moving with V, whereas $\mathbf{u}^-=(\mathbf{u}-\mathbf{v})$, and $\mathbf{u}^+=(\mathbf{u}+\mathbf{v})$. Sources of sound enclosed by S affect the noise field outside of it only through surface integral terms, whereas the effect of sources external to S is taken

into account also through the field integral contribution (in addition to the indirect influence through their effects on the surface integrand terms).

Considering a body in steady conditions, for the surface S large enough to enclose the relevant field noise sources generated by its motion and rigidly connected with it, the external acoustic field may be described by the following, small perturbation, reduced form of Eq. 2

$$p'(\mathbf{x},t) = -\rho_0 \int_S \left[(\mathbf{u}^- \cdot \mathbf{n}\,\mathbf{u} + \mathbf{u} \cdot \mathbf{n}\,\mathbf{v}) \cdot \nabla \hat{G} \right]_\vartheta \mathrm{d}S(\mathbf{y}) - \int_S \left[(p - p_0)\,\mathbf{n} \cdot \nabla \hat{G} \right]_\vartheta \mathrm{d}S(\mathbf{y}) \tag{3}$$

In the following, this boundary integral representation is numerically applied for the prediction of noise generated by a marine propeller in open water in steady axial motion, and a horizontal-axis wind turbine in axial flow, through implementation of a zero-th order panel method for discretization. solution.

3. Numerical Results

Before presenting the predictions of acoustic signatures obtained for a horizontal-axis wind turbine and a marine propeller in steady-flow conditions, the proposed boundary-integral formulation for porous surfaces is validated for elementary noise sources.

These concern the comparison of analytical solutions and numerical predictions from Eq. 3 for acoustic fields generated by a pulsating velocity potential monopole in prescribed motion; in addition, pressure disturbances due to a vortex ring in roto-translation are considered in order to discuss some issues related to the placement of the porous surface.

Monopoles

A pulsating monopole in rectilinear and helicoidal motion is considered, and the corresponding aeroacoustic fields given by analytical solutions are compared with those given by application of the boundary integral approach presented above, for a cylindrical porous surface, S, with axis parallel to the monopole trajectory and to the axis of the helicoidal trajectory, respectively. In both cases, the same motion of the surface is considered, such that the monopole velocity vector is fixed with respect to it. Specifically, the analytical monopole potential field is used to determine the pressure disturbance at prescribed observer positions (via Bernoulli's equation), as well as surface data for the boundary integral approach.

Assuming fluid density equal to $1000\ kg/m^3$, speed of sound equal to $1400\ m/s$, monopole axial velocity and pulsating frequency equal to $20\ m/s$ and $75\ rad/s$, respectively, for the monopole moving along the axis of the cylindrical surface, S, having length equal to $1.82\ m$ and diameter $D = 0.75\ m$, Fig. 1 shows the root mean square (rms) of the induced pressure on it, whereas Fig. 2 presents the rms of the pressure induced by the monopole in helicoidal motion with azimuth velocity equal to $\omega = 37.5\ rad/s$. Then, Figs. 3 and 4 compare the analytical acoustic pressure with the signals predicted by the boundary integral approach, for a near-field observer placed on the same plane of the monopole orthogonal to the cylinder axis, at a radial distance of $0.675D$, for the monopole in rectilinear and helicoidal motion, respectively. The same comparisons for a co-planar, far-field observer at a radial distance of $500D$ are depicted in Figs. 5 and 6. Both observers are in rectilinear motion with the same velocity of the monopole.

The excellent agreement between analytical results and predictions by the integral formulation demonstrates the capability of the porous surface approach to evaluate the acoustic disturbance produced by internal sources.

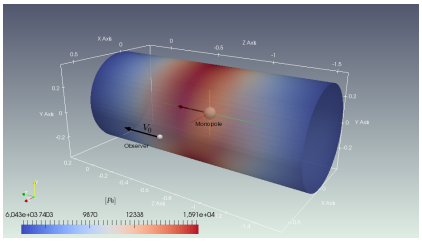

Figure 1: Monopole in rectilinear motion: P_{rms} on S.

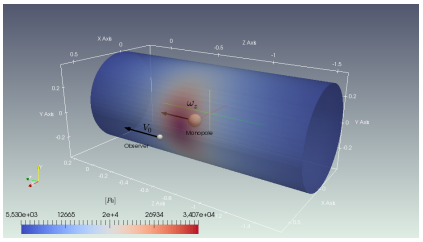

Figure 2: Monopole in helicoidal motion: P_{rms} on S.

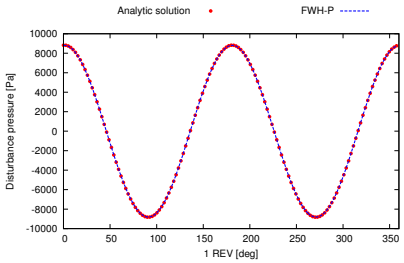

Figure 3: Monopole in rectilinear motion: near field noise.

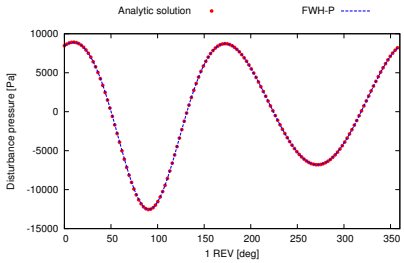

Figure 4: Monopole in helicoidal motion: near field noise.

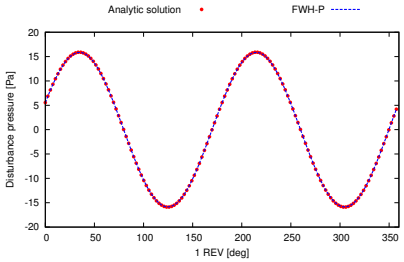

Figure 5: Monopole in rectilinear motion: far field noise.

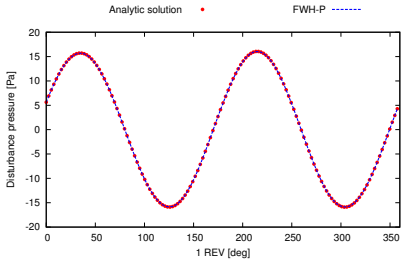

Figure 6: Monopole in helicoidal motion: far field noise.

Vortex-ring

Let us consider a rectangular vortex-ring, of length $1.57\ m$, placed in a meridian plane of the cylindrical surface and rigidly connected with it, that moves with axial velocity equal to $100\ m/s$ and angular velocity around the axis of S equal to $\omega = 37.5\ rad/s$. The outer pressure field and the input data for the integral formulation are computed analytically through the application of the Biot-Savart law and the Bernoulli equation.

For the vortex-ring completely enclosed within the porous surface, Fig. 7 compares the analytical solution and that from Eq. 3, for the observer $obs2$ co-translating with the surface and located at a central section of it, with radial distance D with respect to the surface axis (see Fig. 8). The agreement is excellent, thus confirming the capability of the integral formulation presented to predict the outer acoustic disturbance due to internal sources.

It is of interest to observe the effect on acoustic predictions of a porous surface that encloses only a portion of the vortex (whose filaments parallel to the cylinder axis, therefore, intersect the outflow disk): this configuration resembles the application of the porous surface to a propeller for which, unavoidably, the downstream closure intersects the wake vortices. This is obtained by the introduction of the vortex-ring of length $3\ m$ depicted in Fig. 8, along with the porous surface and the rms of the induced pressure. Figure 9 shows that, for a downstream observer ($obs3$ in Fig. 8) close to the surface end disk, the numerical prediction is badly correlated with the analytical one, whereas a good agreement is observed for an upstream observer ($obs1$ in Fig. 8) close to the surface front disk, as depicted in Fig. 10. A similar quality of results is obtained removing the contribution of the outflow disk (FWH-P$_{w/o}$ curves). The good quality of predictions on upstream observers is due to the weak effect of downstream sources on upstream pressure field. In principle, the inclusion of the

outflow disk implies that only the acoustic effect of the inner vortex portion is taken into account (the influence of the external portion via the porous surface is null), whereas the exclusion of it implies that an approximated effect of the entire vortex is taken into account: therefore, these represent two different approximations, both unsuited for downstream observers. However, note that when the vortex is cut by the outflow disk two additional issues have to be considered: numerical inaccuracy of the disk contribution due to singularities that may arise, and numerical inaccuracy introduced by truncated vortices not complying with conservation laws.

These last considerations suggest that for a porous surface not embedding a whole vortex-ring, a suited solution is to split the ring into two closed contributions separated by an infinitesimal axial distance, as depicted in Fig. 11, where the inner vortex is completely enclosed by S, whereas the outer ring is fully outside of it. In this case, for a given extension of the porous surface, the integral formulation captures all the acoustic effect due to the inner ring, being zero the acoustic effects induced by the outer one through its contributions on S. This is shown in Fig. 12 where, for the downstream observer, the analytical solution obtained by considering the whole vortex perfectly matches with that given by the sum of the analytical contribution from the outside closed ring (R_{ext}) and that from the interior vortex predicted the integral formulation (FWHE-P).

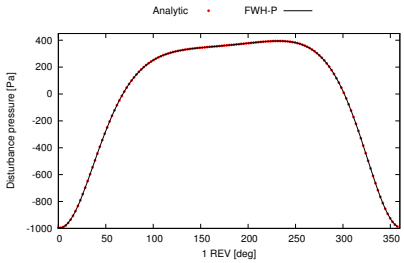

Figure 7: Noise at $obs2$ observer, vortex enclosed by S.

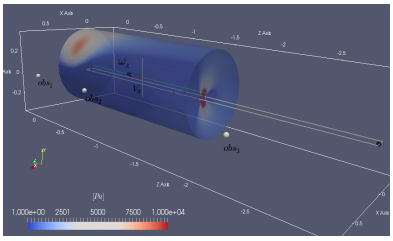

Figure 8: Vortex crossing S: contour plot of P_{rms}.

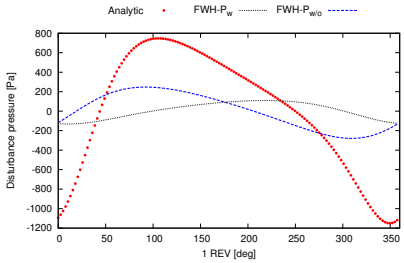

Figure 9: Noise at $obs3$ observer, vortex crossing the outflow disk.

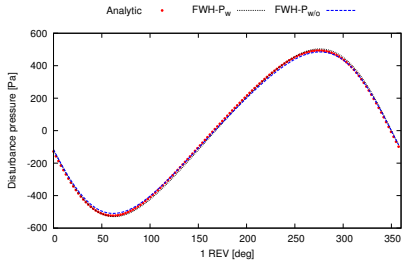

Figure 10: Noise at $obs1$ observer, vortex crossing the outflow disk.

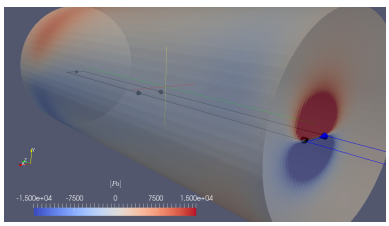

Figure 11: Inner and outer closed vortices, and P_{rms} contour.

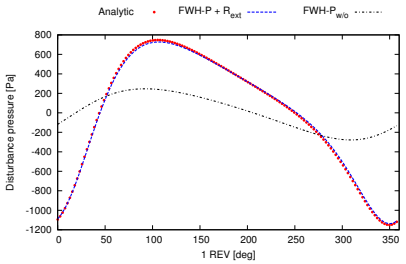

Figure 12: Noise at downstream observer, sum of closed inner and outer vortices.

Wind turbine

Next, a more complex problem consisting of the aeroacoustic analysis of a horizontal axis wind turbine model in uniform onset flow is examined. Aerodynamic input data are provided by a RANS

simulation using the Spalart and Allamaras one equation closure model. The accuracy of CFD aerodynamic results has been proven in [8] through comparisons with experimental data that include blade airloads and downstream velocity field within a 5-diameter length domain behind the rotor disk. The rotor diameter is $D = 0.9\ m$, whereas the operating conditions are defined by tip-speed ratio $\lambda = \omega D/2\, U_\infty = 6$, corresponding to angular velocity $\omega = 133.33\ rad/s$, and undisturbed wind speed $U_\infty = 10\ m/s$. The Reynolds number considered is $Re = 1.036\ 10^5$. The mesh is composed of many patched and partially overlapped structured blocks, with those closer to the blades assuring fine resolution of the wake portion closer to the tip and root. More details are found in [8].

For effective application of the FWHE-P formulation, the porous surface must enclose all of the volume sources of noise; thus, a prior analysis of the spatial distribution of the Lighthill stress tensor is addressed. To this aim, introducing the $L2$ norm of the Lighthill stress tensor, Fig. 13 depicts the iso-surface $L2 = 0.35$, while Fig. 14 shows the iso-surface of the vorticity field: RANS simulation soon becomes inherently inadequate for aeroacoustic purposes because, despite the relevant role played by vorticity and turbulence, these are not captured just one diameter behind the rotor disk.

Although these CFD data are unsuited for an accurate evaluation of the aeroacoustic field, for the scope of this paper a comparison between the pressure signals predicted by the porous formulation and those directly obtained by the CFD solver is anyway presented. Three closed porous cylindrical surfaces having diameter equal to $1.25D$ and lengths $2D$, $3D$, $4D$, respectively, fixed with the turbine blades are considered. The comparison is shown for three acoustic observers, $Obs1$, $Obs2$, $Obs3$ located at radial position $0.75D$ from the cylinder axis, and at axial positions $x = -0.25D$, $x = 0$ and $x = 0.75D$, for $x = 0$ denoting the rotor disk plane. As depicted in Figs. 15, 16 and 17 for all of the observer locations considered, and for all of the surface lengths the agreement betwen CFD and FWHE-P results is very good: indeed, even the 2D-length surface is capable of accurately capture the signals in that enclosing the noise sources generated by the CFD solver.

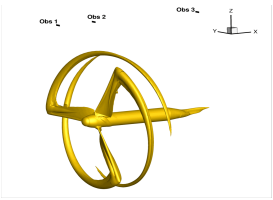

Figure 13: Iso surface $L2 = 0.35$ of Lighthill stress tensor.

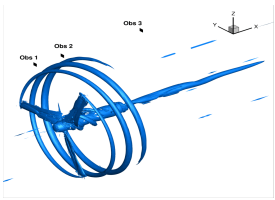

Figure 14: Tip vortices identified by Jeong's criterion also known as $\sigma 2$ criterion.

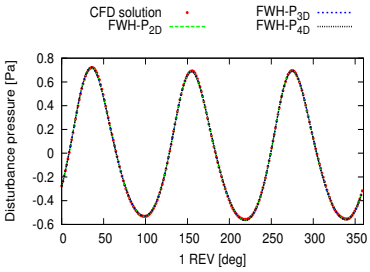

Figure 15: Noise at Obs1.

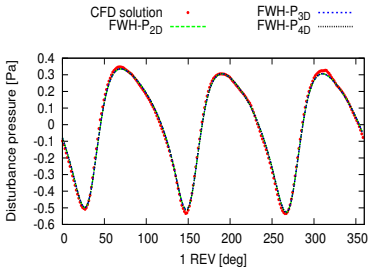

Figure 16: Noise at Obs2.

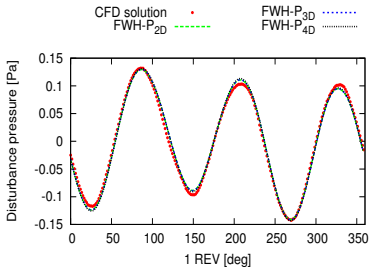

Figure 17: Noise at Obs3.

Marine propeller

The hydroacoustics of INSEAN E779A four-bladed marine propeller in open water, moving at advance ratio $J = 0.88$ is investigated. The propeller diameter is $D = 0.22\ m$, the angular velocity $1500RPM$, whilst the translating velocity is $U_\infty = 5\ m/s$. Four hydrophones placed $0.75D$ far from the propeller shaft and axially located one diameter upstream ($Observer1$), over the propeller disk ($Observer2$), one and two diameters downstream ($Observer3$ and $Observer4$), are considered.

The hydrodynamic input data on S are given by a DES simulation capable to capture the vortex structures downstream the rotor disk, thus avoiding numerical dissipation that may filter out relevant contributions to the overall generated noise. Details of the CFD computation are found in [9]. Two different porous surfaces, open and closed, are used (both fixed in the rotating blade space): one of length $2.75D$ located close to the finest grid zone, the second of length $3.75D$, enclosing the zone where the main spatial variations of the Lighthill stress tensor are present.

Figures 18 and 19 depict the porous surfaces, S, considered in the integral formulation, hydrophone locations, and Lighthill stress tensor $L2$ norm distribution and iso-surface $L2 = 0.0035$. Figures 20, 21, 22, show that the acoustic signals at the first three hydrophones predicted by CFD and FWHE-P approaches are in very good agreement, independently on the kind of porous surface considered. For these observers, the contribution from the downstream end-cap is negligible and, also in the absence of it, the open cylinders well capture the acoustic contribution. In contrast, the shorter surface is unsuited for $Observer4$, neither closed nor open, as demonstrated in Fig. 23. For this downstream observer, and for given extension of S, leaving not-negligible downstream sources of sound outside of the closed surface, or leaving open the surface S, thus virtually ignoring the contribution of a (open) closing surface, S^+, such that $S \cup S^+$ would surround the whole set of sound sources, produce similar drawbacks in the predicted acoustic disturbance. Very good correlation between CFD and FWHE-P results is given by the longest porous surface, with or without downstream closing end-cap.

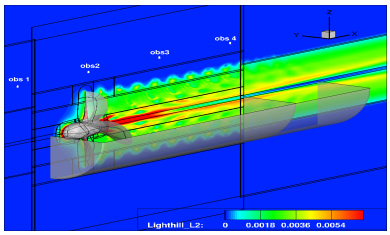

Figure 18: FWH-P surface, field colored by non dimensional $L2$ norm of Lighthill stress tensor

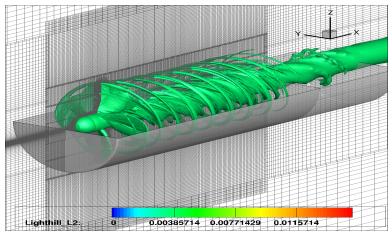

Figure 19: Frobenius norm iso-surface of non dimensional Lighthill stress tensor $_{L2} = 0.0035$

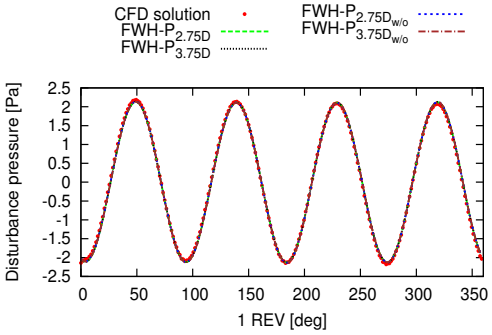

Figure 20: Observer 1, comparison without mean time value.

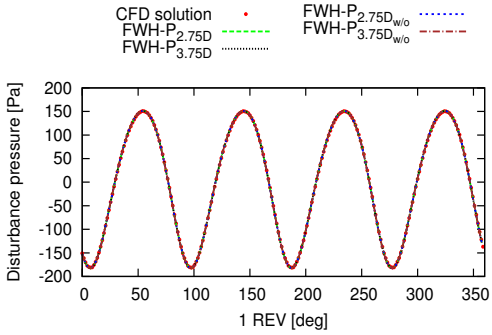

Figure 21: Observer 2, comparison without mean time value.

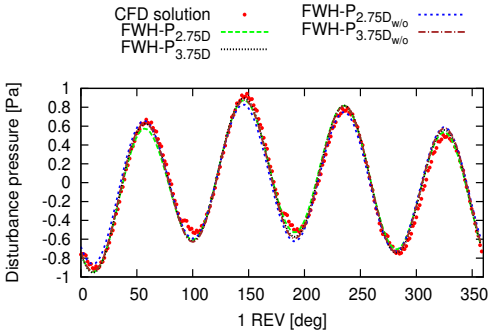

Figure 22: Observer 3, comparison without mean time value.

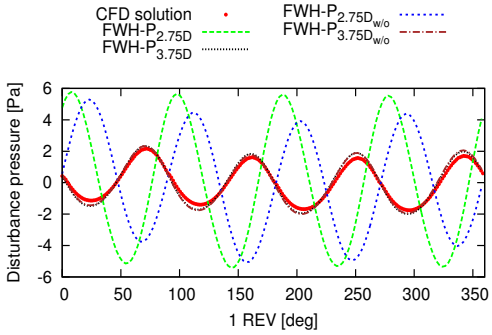

Figure 23: Observer 4, comparison without mean time value.

4. Conclusions

A boundary integral formulation based on the Ffowcs Williams and Hawkings Equation for porous surfaces has been applied to the acoustic analysis of simplified configurations (moving monopoles and vortex-rings) and rotating-wing devices of industrial interest (wind turbines and propellers). Pressure and velocity fields upon the surface have been obtained by analytical solutions for the simplified acoustic sources, whereas CFD simulations have been used for the analyses of rotating-wing devices. For the assessment of the integral formulation proposed, its acoustic solutions are compared with analytical or CFD pressure disturbance predictions. The following considerations may be drawn:

- when the porous surface encloses all of the sound sources present in the field, the external acoustic field is predicted with excellent accuracy, thus proving that this is a viable approach for avoiding the evaluation of computationally expensive volume integrals, when field noise sources are relevant (like, for instance, for transonic or cavitating configurations);
- for practical application of engineering interest, typically some sound sources are left outside of the porous surface (as for the farthest downstream portion of rotating blade wakes): it has been proven that, at least for the cases examined, including or excluding the contribution of the end-cap of the surface introduces different approximations but similar levels of prediction inaccuracy;
- inaccuracy introduced by leaving sound sources outside of the porous surface depends on the location of the considered observer with respect to them;
- CFD data suitable for FWHE-P formulations must avoid numerical diffusion inducing excessive smoothing of downstream vortices strength: in view of this, RANS data are inadequate, whereas DES data are well suited if the convergence of the flow solution is assured in terms of Lighthill stress tensor magnitude.

REFERENCES

1. J.E. Ffowcs Williams, D.L. Hawkings, “Sound Generated by Turbulence and Surfaces in Arbitrary Motion”, *Philosophical Transactions of the Royal Society*, Vol. A264, 1969, pp. 321-342.

2. Philip J. Morris, Lyle N. Long and Kenneth S. Brentner, AN AEROACOUSTIC ANALYSIS OF WIND TURBINES, *42nd AIAA Aerospace Sciences Meeting*, Exhibit 5 - 8 January 2004, Reno, Nevada AIAA 2004-1184

3. S. Ianniello, R. Muscari, and A. Di Mascio, "Ship underwater noise through the acoustic analogy Part I: Nonlinear analysis of a marine propeller in a uniform flow", *J. Mar. Sci. Tech.*, 18, 547-570, 2013.

4. P. Di Francescantonio, A New Boundary Integral Formulation for the Prediction of Sound Radiation, *J. Sound Vib.*, 202, 4 (1997) 491–509.

5. Zane Nitzkorski and Krishnan Mahesh, A dynamic end cap technique for sound computation using the Ffowcs Williams and Hawkings equations, *PHYSICS OF FLUIDS*, 26, 115101 (2014)

6. L. Morino, M. Gennaretti, "Toward an integration of aerodynamics and aeroacoustics of rotors", *AIAA Paper*, 92-02003, DGLR/AIAA 14th Aeroacoustic Conference, Aachen, Germany, May 1992.

7. M. Gennaretti, C. Testa, A Boundary Integral Formulation for Sound Scattered by Elastic Moving Bodies, *J. of Sound and Vibration*, 314, 3-5 (2008) 712-737.

8. S. Zaghi, R. Muscari, A. Di Mascio, Assessment of Blockage effects in Wind Tunnel Testing of Wind Turbines, *Journal of Wind Engineering and Industrial Aerodynamics*, 154:1–9, 2016.

9. R. Muscari, A. Di Mascio and R. Verzicco. Modeling of vortex dynamics in the wake of a marine propeller. *Computers & Fluids*, **73**:65-79, 2013.